Propagation of Joint Space Quantization Error to Operational Space Coordinates and Their Derivatives

Nick Colonnese and Allison M. Okamura, *Fellow, IEEE*

***Abstract*—Many robotic systems achieve position sensing through the use of optical encoders that specify the rotary position of a joint to a certain resolution. Encoders effectively quantize joint space coordinates, and in the process, introduce error. This error propagates to operational space coordinates, limiting position and orientation resolution, and also to operational space coordinate derivative estimates, manifesting as noise that can vitiate the signal. In this paper, we present a characterization of encoder error in a robot system: given encoder specifications, robot kinematics, and a digital filter mapping an operational space coordinate to an estimate of its derivative, the error in joint and operational space coordinates, as well as operational space coordinate derivatives estimates, is described. The error is described for two cases. The first is a general case establishing worst-case bounds. The second case, which models quantization as an additive independent pseudo-quantization-noise source, establishes stochastic metrics on the error. The classic example of quantization error on velocity and acceleration signals for robot operational space coordinates is presented. Simulation and experimental data with a Phantom Premium support the theory presented. These results are intended as a design tool for robot kinematic and feedback control system design.**

***Index Terms*—encoder noise, digital velocity and acceleration estimation**

I. Introduction

FOR many robotic systems position sensing is achieved through the use of an optical encoder in which the rotary position of a joint is specified. Encoders can feature higher reliability and precision at a lower cost compared to other positioning sensing alternatives, which along with their ease of implementation, make them by far the most common position sensing in robotics. The output of an optical encoder is a digital signal, free of external noise, that corresponds to a certain range that the position of the joint lies. Because encoders specify the position of a joint to a limited resolution only, the quantization interval of the encoder, they effectively quantize joint space coordinates, and in the process introduce error. This usually small error propagates to coordinates derived from joint space, operational space, such as Cartesian position or Euler angles. This error propagates further, and can be amplified a great deal, to functions of operational space coordinates, such as estimates of their derivatives, e.g., Cartesian velocity or acceleration.

The authors are with the Mechanical Engineering Department, Stanford University, Stanford, CA, 95305 USA e-mail: (ncolonnese@stanford.edu; aokamura@stanford.edu).

In robot applications such as such as pick and place, soldering or welding, haptic virtual environments, teleoperation, and many others, the position or orientation of the robot must be controlled precisely for high performance. High performance in these applications is commonly achieved using feedback control, which relies directly on the position, and also indirectly, on velocity. The velocity signal, which must be obtained in real time, is usually estimated directly from the quantized position and high fidelity time measurements. Rarely, acceleration is also desired for control, or applications such as inertia compensation or system identification. The error that is initially introduced by quantization in joint space will manifest as "noisy" operational space coordinates, e.g. Cartesian velocity or acceleration. The error on these signals can be a limiting factor in feedback control system design, in which there exists a trade-off between bandwidth, stability, and noise rejection. For example, in a classic robotic teleoperation control scenario, a master and slave robot are linked through a "virtual coupling" to ensure tracking. Both position and velocity information is required for each robot, and these signals need to be sufficiently smooth for good performance. A characterization of the noise on these signals, whose source is quantization, would be valuable in designing the physical architecture of the robots, i.e., appropriate encoders, link lengths, gear ratios, etc., as well as feedback control structure.

It is true that velocity and acceleration signals can be obtained using additional sensors, such as a tachometer for velocity, and accelerometers for acceleration, however, these sensors face different challenges. Understanding encoder quantization error could highlight situations in which these other sensors are expected to have superior or inferior performance.

Past researchers have explored quantization from optical encoders on joint space derivatives. Resolution of estimates for velocity and acceleration was developed by Tanaka et al. [1]. Harrison and McMahon analyzed signal-to-noise SNR values for finite-difference-method estimates on velocity and acceleration estimates [2], which was expanded by Harrison and Stoten [3]. Kavanagh explored quantization error on velocity estimates is in [4]. Explicit variances from the output of recursive filters was explored by Mollova for recursive cascaded digital filters, [5].

There has been extensive research on quantization error for analog to digital, A/D, converters. These include Bennet, Gray, Sripad, Widrow, and Kollar. (I need to spend more time reading this literature to give a quick lit review).

Past researchers have proposed many methods to estimate

velocity and acceleration from quantized position. The techniques can loosely be separated into finite difference, (or "fixed-time") and low-pass filters algorithms, [3], [6], [7], inverse time, (or "fixed-displacement"), methods, [8], Kalman Filters, either fixed ,[9], [10],or adaptive, [11], and adaptive window techniques, [12], [13], [14], [15], [16].

In this paper we analyze quantization error on joint space coordinates, provide a description of how this error propagates to operational space coordinates, and then show how this error propagates further to estimates of operational space derivatives. The results for the error introduced by quantization are for two cases. The first case, which is applicable generally, establishes "worst-case" bounds for the error on the various signals given a configuration of the robot. The second case, which models quantization error as additive white noise, establishes error distribution metrics for the various signals, .i.e., means and variances for a given configuration. Conditions for which quantization may be modeled as additive white noise are established.

The contribution of this work is to characterize quantization error in robotic systems as a design tool. The results presented are intended to inform robot mechanical and control system design by providing a method to predict the effect of quantization error. In this way, a robot designer can select appropriate encoders, link lengths, gear ratios, etc., for a given sensing performance. For the feedback control system designer, the effect of the quantization error on the position control algorithm can be found. With bounds on the the structure of the control algorithm established to yield acceptable error, meaning constraints on noise rejection, and design for other objectives, such as accordingly.

The organization of the paper is as follows. First a system model representing quantization in joint space from optical encoders is presented. Then a general procedure to characterize encoder error in a robotic system, meaning error in joint space, operational space, and derivatives in operational space, is explained. Then the effect of various parameters of the common finite difference method, FDM, and low-pass filter algorithm on quantization error are analyzed. Simulated and experimental data is presented in VI validating the theory presented.

II. Notation List

Table I is a list for the notation used.

III. System Model

The system we consider is given in Fig. 1. Discrete-time true joint space coordinates $\theta_1, \theta_2, \ldots, \theta_n \in \mathbf{R}$ undergo spatial quantization with respective quantization intervals $\Delta_1, \Delta_2, \ldots, \Delta_n \in \mathbf{R}$ resulting in quantized joint angles $\hat{\theta}_1, \hat{\theta}_2, \ldots, \hat{\theta}_n \in \mathbf{R}$. The quantized joint angles are mapped to operational space coordinates $\hat{x}_1, \hat{x}_2, \ldots, \hat{x}_m \in \mathbf{R}$ by the forward kinematics. A derivative signal estimate on an operational space coordinate at index j is obtained through a single-input, single-output, discrete transfer function $H_{(.)}$, where $_{(.)}$ represents the order of the derivative estimate. For example, $\dot{\hat{x}}_j$ is a velocity estimate of $\hat{x}_j$ formed by H_v, and $\ddot{\hat{x}}_j$ an acceleration estimate formed by H_a.

TABLE I
Notation List Table

Symbol	Description
$\Delta_i \in \mathbf{R}$	quantization interval at joint coordinate at index i
$\Delta \in \mathbf{R}^n$	quantization interval vector
$\theta_i \in \mathbf{R}$	true joint space coordinate at index i
$\hat{\theta}_i \in \mathbf{R}$	quantized joint space coordinate at index i
$\tilde{\theta}_i \in \mathbf{R}$	error on joint space coordinate at index i
$\theta \in \mathbf{R}^n$	true joint space coordinate vector
$\hat{\theta} \in \mathbf{R}^n$	quantized joint space coordinate vector
$\tilde{\theta} \in \mathbf{R}^n$	error on joint space coordinate vector
$x_j \in \mathbf{R}$	true operational space coordinate j
$\hat{x}_j \in \mathbf{R}$	quantized operational space coordinate j
$\tilde{x}_j \in \mathbf{R}$	error on operational space coordinate j
$x \in \mathbf{R}^m$	true operational space coordinate vector
$\hat{x} \in \mathbf{R}^m$	quantized joint space coordinate vector
$\tilde{x} \in \mathbf{R}^m$	error on joint space coordinate vector
$\bar{x} \in \mathbf{R}^p$	state space realization vector of H
$\sigma^2_{\tilde{\theta}_i} \in \mathbf{R}$	joint space error var. at coordinate i
$\sigma^2_{\tilde{x}_j} \in \mathbf{R}$	op. space error var. at coordinate j
$\sigma^2_{\tilde{y}} \in \mathbf{R}$	op. space deriv. error variance
$\Sigma_{\tilde{\theta}} \in \mathbf{R}^{n\times n}$	joint space error covariance matrix
$\Sigma_{\tilde{x}} \in \mathbf{R}^{m\times m}$	op. space error covariance matrix
$\Sigma_{\bar{x}} \in \mathbf{R}^{p\times p}$	extended state covariance matrix
$J \in \mathbf{R}^{m\times n}$	Jacobian matrix, $\dot{x} = J\dot{\theta}$
$J_i \in \mathbf{R}^m$	ith column of J
$a_i \in \mathbf{R}$	coefficients of j.s.c. variances on o.s.c

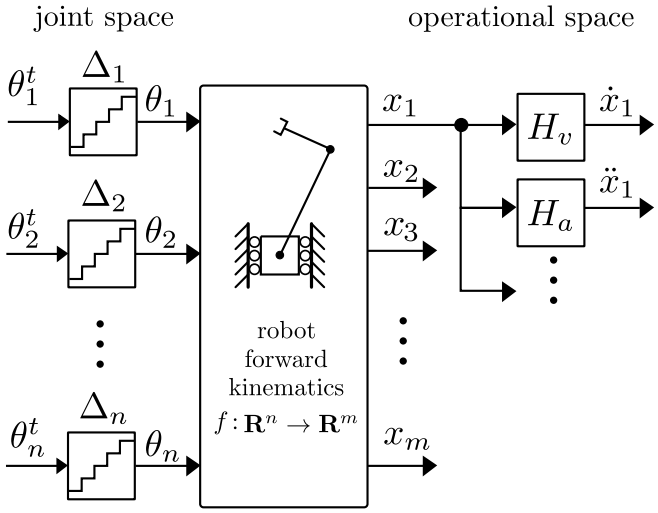

Fig. 1. Caption Here.

IV. Error Propagation

Here we describe the propagation of quantization error on joint space coordinates to operational space coordinates, and then, to estimates of operational space coordinate derivatives. We propose two models for quantization in joint space. The first model is a general one useful for establishing worst-case bounds on the error. The second models each quantization as independent additive pseudo-quantization-noise, (PQN), for

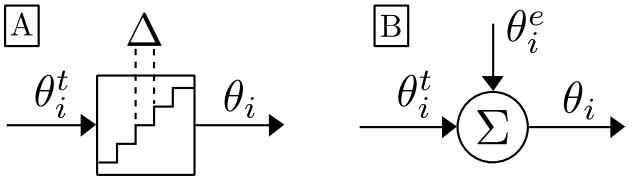

Fig. 2. Two conceptual models for quantization. A: quantization operates on true joint space coordinate at joint i, θ_i^t, and returns θ_i with resolution Δ_i. B: Noise $\theta_i^e \in \mathbf{R}[-\Delta_i/2, \Delta_i/2]$ is added to a true joint space coordinate at joint i, θ_i^t, to produce θ. For cases in which quantization is well approximated by pseudo-quantization-noise, PQN, the noise θ_i^e is uncorrelated with the input signal, white, and uniform between $-\Delta_i/2$ and $\Delta_i/2$.

which stochastic metrics, e.g. means and variances, on the error are determined. Conditions for which the independent PQN model is appropriate are presented in Appendix B.

A. Error in Joint Space

The quantization operator maps an input set with an infinite number of elements to an output set with a finite number of elements. An ideal optical encoder measuring the rotary position of a robot joint behaves as a uniform quantizer in which the output elements are all equally spaced. At a certain joint at index i, quantization operates on the true joint space coordinate, $\theta_i \in \mathbf{R}$, to return a quantized coordinate, $\hat{\theta} \in \mathbf{R}$. The error at this coordinate, $\tilde{\theta}_i \in \mathbf{R}$, is the difference between the quantized and true coordinate,

$$\tilde{\theta}_i = \theta_i - \hat{\theta}_i. \tag{1}$$

Quantization introduces error on the joint space coordinate measurement, which we refer to as "noise". This noise is used as a conceptual model, and should not be confused with some additional source of error. This interpretation is shown in Fig. 2.

At joint index i, the quantized joint coordinate is always within $\Delta_i/2$ of the true joint coordinate. Thus, the error at a joint must satisfy

$$-\frac{1}{2}\Delta_i \leq \tilde{\theta}_i \leq \frac{1}{2}\Delta_i. \tag{2}$$

This can also be expressed in vector form as

$$-\frac{1}{2}\Delta \leq \tilde{\theta} \leq \frac{1}{2}\Delta. \tag{3}$$

where $\tilde{\theta} \in \mathbf{R}^n$ is a vector of the joint space coordinate errors $\tilde{\theta} = \left[\tilde{\theta}_1, \tilde{\theta}_2, \ldots, \tilde{\theta}_n\right]^T$, and $\Delta \in \mathbf{R}^n$ is a vector of the quantization intervals: $\Delta = [\Delta_1, \Delta_2, \ldots, \Delta_n]^T$. Equations (2) and (3) establish worst-case bounds for the quantization error in joint space.

If quantization on a joint space coordinate at index i is modelled stochastically as additive pseudo-quantization-noise, (PQN), then $\hat{\theta}_i$ has a uniform distribution,

$$\tilde{\theta}_i \sim U(-\Delta_i/2, \Delta_i/2). \tag{4}$$

The mean of $\tilde{\theta}_i$, $\mathbf{E}\tilde{\theta}_i$, is given by

$$\mathbf{E}\tilde{\theta}_i = \int \tilde{\theta}_i p(\tilde{\theta}_i) d\tilde{\theta}_i = 0. \tag{5}$$

The variance of $\tilde{\theta}_i$, $\sigma^2_{\tilde{\theta}_i}$, is given by

$$\sigma^2_{\tilde{\theta}_i} = \mathbf{E}(\mathbf{E}(\tilde{\theta}_i - \mathbf{E}\tilde{\theta}_i)\mathbf{E}(\tilde{\theta}_i - \mathbf{E}\tilde{\theta}_i)) = \Delta_i^2/12. \tag{6}$$

For the PQN model, $\tilde{\theta}$ is random vector. The mean of $\tilde{\theta}$, $\mathbf{E}\tilde{\theta}$, is given by

$$\mathbf{E}\tilde{\theta} = \mathbf{0}, \tag{7}$$

where $\mathbf{0}$ denotes the zero vector in $\mathbf{R}^n$.

The covariance of $\tilde{\theta}$, $\Sigma_{\tilde{\theta}} \in \mathbf{R}^{n \times n}$, is defined by

$$\Sigma_{\tilde{\theta}} = \mathbf{E}(\mathbf{E}(\tilde{\theta} - \mathbf{E}\tilde{\theta})\mathbf{E}(\tilde{\theta} - \mathbf{E}\tilde{\theta})^T). \tag{8}$$

If the error at one joint is independent of another, $\Sigma_{\tilde{\theta}}$ is given by the diagonal matrix,

$$\Sigma_{\tilde{\theta}}(i,i) = \frac{\Delta_i^2}{12} \qquad \text{for } i = 1, 2, \ldots, n. \tag{9}$$

B. Local Error in Operational Space

Let $x \in \mathbf{R}^m$ and $\hat{x} \in \mathbf{R}^m$ be vectors representing operational space coordinates formed from true and quantized joint space coordinates, respectively, using the forward kinematics $f : \mathbf{R}^n \to \mathbf{R}^m$. The operational space coordinates error vector, $\tilde{x} \in \mathbf{R}^m$ is defined as

$$\tilde{x} = \hat{x} - x. \tag{10}$$

We use a linear approximation to the forward kinematics to describe local error propagation. Let $J \in \mathbf{R}^{m \times n}$ be the Jacobian relating joint and operational space velocities, $\dot{x} = J\dot{\theta}$. Then

$$\begin{aligned}
\tilde{x} &= \hat{x} - x && (11)\\
&= f(\hat{\theta}) - f(\theta) && (12)\\
&\approx f(\theta) + J(\hat{\theta} - \theta) - f(\theta) && (13)\\
&= f(\theta) + J(\theta + \tilde{\theta} - \theta) - f(\theta) && (14)\\
&= J\tilde{\theta} && (15)
\end{aligned}$$

The linear approximation of $f(\hat{\theta})$, performed at θ, is valid if the contribution of higher-order terms in $\hat{\theta} - \theta$ are negligible compared the affine and linear terms. The $J(\hat{\theta} - \theta)$ term scales linearly with the entries of $\hat{\theta} - \theta$, while the higher-order terms scale quadratically or higher. The entries of $\hat{\theta} - \theta$ are bounded by the quantization interval Δ_i for each joint, and if the quantization intervals are sufficiently small, the approximation is valid. However, because the Jacobian is configuration dependent, the approximation is only valid locally, in the neighborhood of values close to θ.

The error at operational space coordinate indexed by j, $\tilde{x}_j \in \mathbf{R}$, must satisfy

$$-\sum_{i=1}^{n} \frac{|J_{ji}|}{2}\Delta_i \leq \tilde{x}_j \leq \sum_{i=1}^{n} \frac{|J_{ji}|}{2}\Delta_i, \tag{16}$$

or in vector form,

$$-\frac{|J|}{2}\tilde{\Delta} \leq \tilde{x} \leq \frac{|J|}{2}\tilde{\Delta}, \tag{17}$$

where $|J|$ is the element-wise absolute value of J. Equation (17) establishes a worst-case bound.

For the independent PQN model of quantization, a local description of the mean of the error vector in operational space is given by

$$\mathbf{E}\tilde{x} = \mathbf{0}, \tag{18}$$

where $\mathbf{0}$ represents the zero vector in $\mathbf{R}^m$. The local description of the covariance of the error vector in operational space is given by

$$\Sigma_{\tilde{x}} = J\Sigma_{\tilde{\theta}}J^T. \tag{19}$$

The variance of a specific operational space coordinate at index j, $\sigma^2_{\tilde{x}_j}$ is given by the (j,j) entry of $\Sigma_{\tilde{x}}$,

$$\sigma^2_{\tilde{x}_j} = \Sigma_{\tilde{x}}(j,j). \tag{20}$$

Because

$$\sigma^2_{\tilde{x}_j} = (J\Sigma_{\tilde{\theta}}J^T)(j,j) \tag{21}$$

$$= \left(\sum_{i=1}^{n} J_i J_i^T \frac{\Delta_i^2}{12}\right)(j,j) \tag{22}$$

$$= \sum_{i=1}^{n} \frac{\Delta_i^2 a_i}{12}, \tag{23}$$

where

$$a_i \in \mathbf{R} = J_i J_i^T(j,j), \tag{24}$$

and J_i is the ith column of J. Equation (22) establishes that given a certain configuration of the robot, the variance of the error on an operational space coordinate is a linear combination of the square of the quantization intervals Δ_i^2. This representation is useful because the set of a_i for $i = 1, 2, \ldots, n$ show the relative effect of the quantization intervals on an operational space coordinate error.

C. Error Propagation to Derivative Signals

Consider a single-input, single-output, discrete transfer function H with operational space coordinate at index j, $\hat{x}_j$, as its input, and $\hat{y} \in \mathbf{R}$, as its output. The output of the transfer function will be the superposition of the true operational space coordinate and the error on the coordinate propagated through the transfer function. Here we are interested in transfer functions mapping an operational space coordinate to an estimate of one of its derivatives, although the approach is applicable to any transfer function.

For a *given* error on the operational space coordinate at index j, $\tilde{x}_j$, the error on the derivative signal, $\tilde{y}$, is propagated through the transfer function. This is useful for establishing a worst-case bound for the derivative signal error. Because $\tilde{x}_j$ is bounded by Equation (16), and if the transfer function is stable, $\tilde{y}$ is also be bounded. The derivative signal error, satisfies

$$\|\tilde{y}\|_\infty = \|H(\tilde{x}_j)\|_\infty \tag{25}$$

$$\leq \|H\|_{l1}\|\tilde{x}_j\|_\infty, \tag{26}$$

where $\|\tilde{y}\|_\infty$, $\|H(\tilde{x}_j)\|_\infty$, and $\|\tilde{x}_j\|_\infty$ are the infinity norms of the discrete time signals, i.e., the peak absolute value, and $\|H\|_{l1}$ is the l_1 norm of the transfer function H. Equation (26) establishes the worst-case contribution of the error on the operational space coordinate to an estimate of one of its derivative signals.

Results for the average error on the derivative signal are obtained by examining the stochastic error of the operational space coordinate, which is is valid for the independent PQN model of quantization. Because the input error to the transfer function, $\tilde{x}_j$, is zero mean, the mean of the output, $\sigma^2_{\tilde{y}}$, is also zero mean.

$$\mathbf{E}\tilde{y} = 0. \tag{27}$$

For the independent PQN model, the input error is stationary white noise with zero mean, and if the transfer function H is stable, the output variance will tend to a steady-state value given by

$$\sigma^2_{\tilde{y}} = \|H\|_2^2 \sigma^2_{\tilde{x}_j}, \tag{28}$$

where $\|H\|_2^2$ is the squared H_2 norm of the transfer function.

Consider the standard state-space form (A, B, C, D) representation of H, and let $\bar{x} \in \mathbf{R}^p$ be the state of the state-space realization of the transfer function H. For clarity, we call $\bar{x}$ the "extended state'' of the operational space coordinate. If H is expressed in standard controller canonical form, the entries of $\bar{x}$ consist of the current and $p-1$ last position values used to determine the next output. We let the error on the operational space coordinate be $e \in \mathbf{R}$. Then, the state space equation mapping position to derivative signal with input error is

$$\bar{x}_{k+1} = A\bar{x}_k + Be_k \tag{29}$$

$$y_{k+1} = C\bar{x}_k + De_k. \tag{30}$$

Let $\sigma_e^2 \in \mathbf{R}$ be the variance of the error in operational space at a certain coordinate. The value of σ_e^2, (in a specific configuration), can be found using the methods from the previous subsection. For example, if the first operational coordinate was of interest, $\sigma_e^2 = \sigma^2_{x_j^e} = \Sigma_{x^e}(1,1)$.

Noting that the mean of the extended state is zero, the covariance of the extended state at time k is

$$\Sigma_{\bar{x}(k)} = \mathbf{E}\bar{x}(k)\bar{x}^T(k). \tag{31}$$

Because

$$\bar{x}(k+1) = A\bar{x}(k) + Be(k), \tag{32}$$

the covariance of the extended state at time $k+1$ is

$$\Sigma_{\bar{x}}(k+1) = \mathbf{E}\bar{x}(k+1)\bar{x}^T(k+1) \tag{33}$$

$$= \mathbf{E}(A\bar{x}(k) + Be(k))(A\bar{x}(k) + Be(k))^T \tag{34}$$

$$= A\Sigma_{\bar{x}(k)}A^T + B\sigma_e^2 B^T. \tag{35}$$

From equations (34) to (35), the other terms vanish because the error is zero mean. With this result the transient development of the extended state covariance can be found for a given initial condition on the error covariance. However, if the filter H is stable, and the error covariance is constant, then the extended state covariance will tend to a steady-state value that can be determined by setting

$$\Sigma_{\bar{x}}(k) = \Sigma_{\bar{x}}(k+1) = \Sigma_{\bar{x}}(\infty), \tag{36}$$

and solving

$$\Sigma_{\bar{x}} = A\Sigma_{\bar{x}}A^T + B\sigma_e^2 B^T. \tag{37}$$

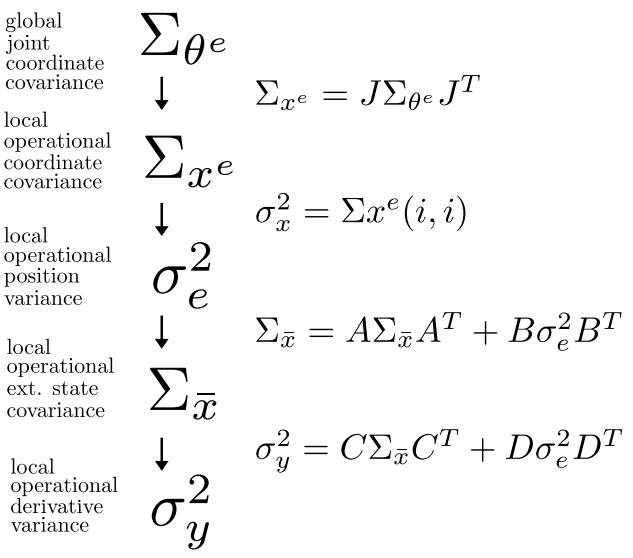

Fig. 3. A schematic of the process of determining operational space derivative signal variance from quantization in joint space. First, from the quantization intervals the error covariance in joint space position, Σ_{θ^e}, is defined. For a certain configuration of the robot, the error covariance on operational space position, Σ_{x^e}, can be obtained from the error covariance in joint space position and the Jacobian. Then, the variance of a specific operational space position error can be extracted from error covariance matrix to get σ_e^2. Using the state space realization matrices (A, B, C, D) defined by the transfer function H mapping operational space position to the derivative signal, the covariance of the state space realization vector, $\Sigma_{\bar{x}}$, can be solved for. Finally, the error covariance on the operational space derivative, σ_y^2, is determined.

TABLE II
NOMINAL FILTER PARAMETERS

Space	Quantization Error Model	
	General	Independent PQN
joint	$-\frac{1}{2}\Delta \leq \tilde{\theta} \leq \frac{1}{2}\Delta$	$\mathbf{E}\tilde{\theta} = \mathbf{0}$ $\Sigma_{\tilde{\theta}}(i,i) = \frac{\Delta_i^2}{12}$
operational	$-\frac{\lvert J\rvert}{2}\tilde{\Delta} \leq \tilde{x} \leq \frac{\lvert J\rvert}{2}\tilde{\Delta}$	$\mathbf{E}\tilde{x} = \mathbf{0}$ $\Sigma_{\tilde{x}} = J\Sigma_{\tilde{\theta}}J^T$
op. deriv.	$\lVert\tilde{y}\rVert_\infty \leq \lVert H\rVert_{l1}\lVert\tilde{x}_j\rVert_\infty$	$\mathbf{E}\tilde{y} = 0$ $\sigma_{\tilde{y}}^2 = \lVert H\rVert_2^2\sigma_{\tilde{x}_j}^2$

Space	Quantization Error Model	
	General	Stochastic
joint	$-\frac{1}{2}\tilde{\Delta} \leq \theta^e \leq \frac{1}{2}\tilde{\Delta}$	$\mathbf{E}\theta^e = \mathbf{0}$ $\Sigma_{\theta^e}(i,i) = \frac{\Delta_i^2}{12}$
operational	$-\frac{1}{2}\lvert J\rvert\tilde{\Delta} \leq x^e \leq \frac{1}{2}\lvert J\rvert\tilde{\Delta}$	$\mathbf{E}x^e = \mathbf{0}$ $\Sigma_{x^e} = J\Sigma_{\theta^e}J^T$
op. derivative	$\lVert y^e\rVert_\infty \leq \lVert H\rVert_{l1}\lVert x_j^e\rVert_\infty$	$\mathbf{E}y^e = 0$ $\sigma_{y^e}^2 = C\Sigma_{\bar{x}}C^T + D\sigma_{x_j^e}^2 D^T$

Fig. 4. Caption Here. (I am experimenting with this Figure. I think the summary information is important, but it seems a bit "clunky".

Equation (37) is the discrete Lyapunov equation and can be solved using several methods, [17], [18], [19].

With the extended state covariance, $\Sigma_{\bar{x}}$, and the operational space error variance, σ_e^2, the variance of the derivative signal, $\sigma_{\dot{y}^e}^2$, e.g., the variance of the error on the velocity or acceleration of the operational space coordinate, can be determined by

$$\sigma_{\dot{y}^e}^2 = C\Sigma_{\bar{x}}C^T + D\sigma_e^2 D^T. \tag{38}$$

Fig. 3 gives a schematic for the process of determining an operational space derivative signal variance from quantization in joint space. First, from the quantization intervals the error covariance in joint space coordinates, Σ_{θ^e}, is defined. For a certain configuration of the robot, the error covariance on operational space coordinates, Σ_{x^e}, can be obtained from Σ_{θ^e} and the Jacobian. Then, the variance of the error of a specific operational space coordinate can be extracted from Σ_{x^e} to get σ_e^2. Using the state space realization matrices (A, B, C, D) defined by the transfer function H mapping an operational space coordinate to the derivative signal, the covariance of the state space realization vector, $\Sigma_{\bar{x}}$, can be solved for. Finally, the error covariance on the operational space derivative, $\sigma_{\dot{y}^e}^2$, is determined.

D. Example: Error on Cartesian Velocity of a Planar PRR Robot

Here we apply the methods of this section to estimate the error distribution on the Cartesian velocity of a planar PRR robot from quantization in joint space. This particular example is chosen because real-time velocity estimates constructed from position measurements are commonly desired in practice. Here we use the IPQN model for quantization.

A planar PRR robot with a quantization interval of $2\pi/10000$ rad on its revolute joints, and $l/10000$ on its prismatic joint, a first link length of $2l$, and a second link length of l, has an estimate on its velocity using the common finite difference method and low-pass filter algorithm discussed later in Section V. Two low-pass filters filters are considered: both have a sample rate of 1000 Hz, and a cut-off frequency of 50 Hz, but one filter is first order, and the other is second order. To communicate the error on the operational space Cartesian velocity we define

$$\Sigma_{v^e} = \begin{bmatrix} \sigma_{v_x^e}^2 & 0 \\ 0 & \sigma_{v_y^e}^2 \end{bmatrix}, \tag{39}$$

where $\sigma_{v_x^e}^2$ is the variance of the error in the x direction, and $\sigma_{v_y^e}^2$, the y direction. Note that Σ_{v^e} is not the covariance matrix of the error on velocity vector, which would in general have a non-zero diagonal entry. Σ_{v^e} is defined in this way because the methods presented are for obtaining the variances of the derivative signals errors, and not the covariances. Fig. 5 displays the matrix ellipsoids of Σ_{v^e}, that is, the area in $\mathbf{R}^2$ defined by

$$E(\Sigma_{v^e}, k) = \{(q \in \mathbf{R}^2 | q^T\Sigma_{v^e}^{-1}q \leq k\}, \tag{40}$$

where $k \in \mathbf{R}$ is a constant determining the level set of the ellipsoid. In Fig. 5 the value of k is $75l/s$ for ease of

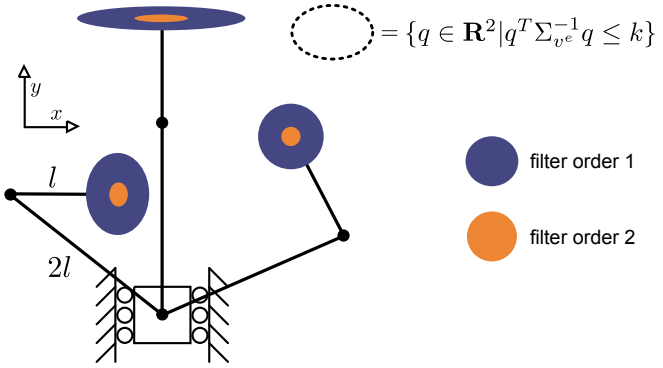

Fig. 5. The matrix ellipsoids of the error on operational space velocity for different configurations of a planar PRR using the finite difference method and low-pass filter algorithm.

visualization. For the configuration on the right the standard deviation of the error is about the same in both directions, with a value of around $.08l/s$ for the first order filter, and $.02l/s$ for the second order filter.

V. Velocity and Acceleration Signals

In this section the error on velocity and acceleration signals is analyzed using the finite difference method, FDM, and low-pass filter scheme. We identify the parameters of the estimation scheme and describe how each affects the error. Here we assume the IPQN model to yield stochastic results for the error.

A. Filter Parameters and Structure

The structure of the filters investigated is shown in Fig. 6. The operational space coordinate (with error) at time step k, $x(k)$, undergoes d back differences, for velocity, $d = 1$, for acceleration, $d = 2$, and so on, and then n first-order low-pass filters with a cut-off frequency of w_0 [rad/s], with unity gain at zero frequency. Other filters could be used; this specific filter was chosen because of its simplicity, and to provide a clear description of how the filter parameters affect error. The generality of the filter results is discussed in Section VII.

Given the filter architecture, the error on the velocity and acceleration depends on four parameters: the variance of error in operational space, $\sigma_{x^e}^2$, (or the standard deviation), the low-pass filter cut-off frequency, f_0, the sample frequency, f, and the filter order, n.

The affect of each parameter on the error distribution of velocity or acceleration is analyzed in Figures 7, 8, and 9 by varying the particular value of a parameter while the others are maintained at a nominal value, except for the filter order, in which filter orders 1, 2, 3 and 4 are included in each plot. The nominal values of the filter parameters are $\sigma_{x^e} = .1$ [mm], $f = 1000$, [Hz], and $f_0 = 50$ [Hz]. Since it has been established in Section IV that the error is zero mean, the following discussion analyzes the standard deviation of the derivative error: σ_{v^e} for the error on velocity, and σ_{a^e} for the error on acceleration. The solid lines represent theory, and the dotted lines that of numerical simulation that is discussed in Section VI.

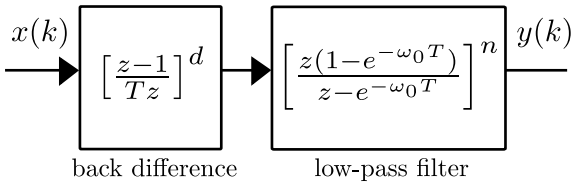

Fig. 6. Filter structure for estimating velocity and acceleration from position. The quantized position $x(k)$ undergoes d back differences (for velocity, $d = 1$, for acceleration, $d = 2$), and then n low-pass filters with a cut-off frequency of w_0 [rad/s] and unity gain at DC.

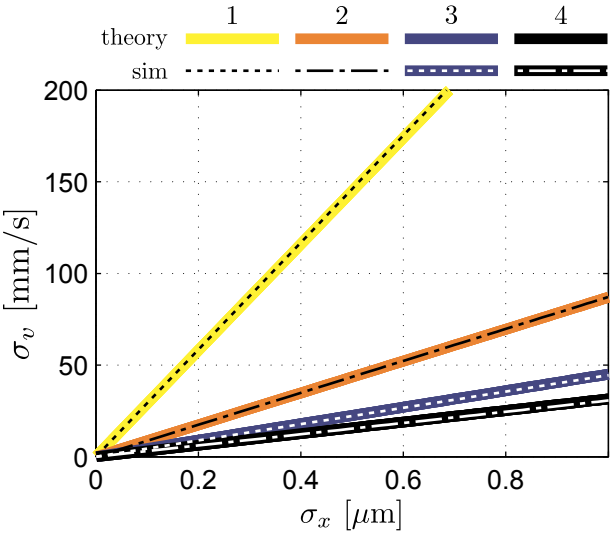

Fig. 7. The standard deviation of the error, σ_v, on the velocity estimate for filter orders n = 1,2,3, and 4, plotted against the standard deviation of the error in operational space position, σ_x. The standard deviation of the error on velocity is linear in σ_x for all filter orders, and monotonically decreases as the filter order is increased. This is the case for higher order derivatives as well.

B. Effect of Parameters on Derivative Error

Fig. 7. displays the standard deviation of the error on velocity, σ_{v^e}, for filter orders n = 1, 2, 3 and 4, plotted against the standard deviation of the error in operational space, σ_{x^e}. The standard deviation of the error on velocity is linear in σ_{x^e} for all filter orders, and monotonically decreases as the filter order is increased. This is the case for higher order derivatives, such as acceleration, as well. From Equation (22) it was established in a certain configuration the variance of the error in operational space is a linear combination of the square of the quantization intervals. This implies that the standard deviation σ_{x^e} is linear in *all* the quantization intervals, as well as σ_{v^e}, meaning that if all the quantization intervals were halved, σ_{x^e} and σ_{v^e} would also be halved.

Fig. 8 shows σ_{v^e} plotted against the cut-off frequency of the low-pass filter, f_0. For much lower cut-off frequencies with respect to the sample rate, the error is roughly linear for all filter orders. For cut-off frequencies close to the sample rate, the difference between the different order filters is minimal, and all filter orders yield approximately the same error. The

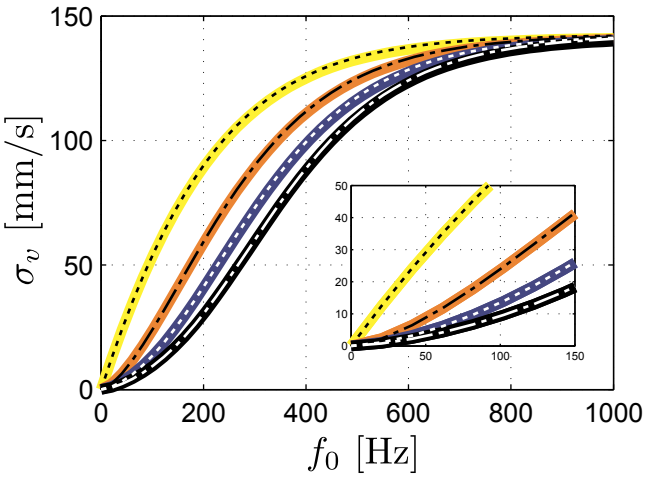

Fig. 8. The standard deviation of the error on velocity plotted against the cut-off frequency of the low-pass filter. For low cut-off frequencies with respect to sample rate, the error is roughly linear for all filter orders. For cut-off frequencies close to the sample rate all filter orders yield approximately the same error.

TABLE III
RELATIONSHIP BETWEEN SAMPLE FREQUENCY AND ERROR

Condition	Error tends to a value as $f \Uparrow$	Error as $f \Uparrow$
$n < d$	no	$\Uparrow$
$n = d$	yes	$\Uparrow$
$n > d$	yes	$\Downarrow$

For sample rate f, derivative order d, and filter order n, when the cut-off frequency, f_0, is less than the Nyquist frequency : $f_0 < f_N = f/2$ [Hz].

same type of behavior is seen for the acceleration error, and higher order derivatives.

Unlike the operational space coordinate error and cut-off frequency, the sample rate's effect on the derivative signal error is different depending on the derivative order of the filter. The following analysis assumes that the cut-off frequency, f_0, is less than the Nyquist frequency: $f_0 < f_N = f/2$ [Hz]. For conditions in which this is not true, the cut-off frequency is aliased, resulting in the actual cut-off frequency not being the designed value. Fig. 9 displays the standard deviation of the error on velocity, σ_{v^e}, and acceleration, σ_{a^e}, plotted against the sample frequency. As the sampling rate increases, σ_{v^e} approaches a value for all filter orders. For a first-order filter, σ_{v^e} increases as the sample rate increases, but decreases for a second order filter or higher. However, unlike σ_{v^e}, for a first order filter, σ_{a^e} does not approach a value as the sampling rate increases; it is linear in the sampling rate. For higher filter orders, however, σ_{a^e} does approach a value. Also, for filter orders 1 and 2 the standard deviation of the error increases with faster sampling, but decreases for third and higher order filters. These results demonstrate a relationship between the sample rate, f, the derivative signal order, d, and the order of the low-pass filter, n. In fact, these results generalize, as summarized in Table III.

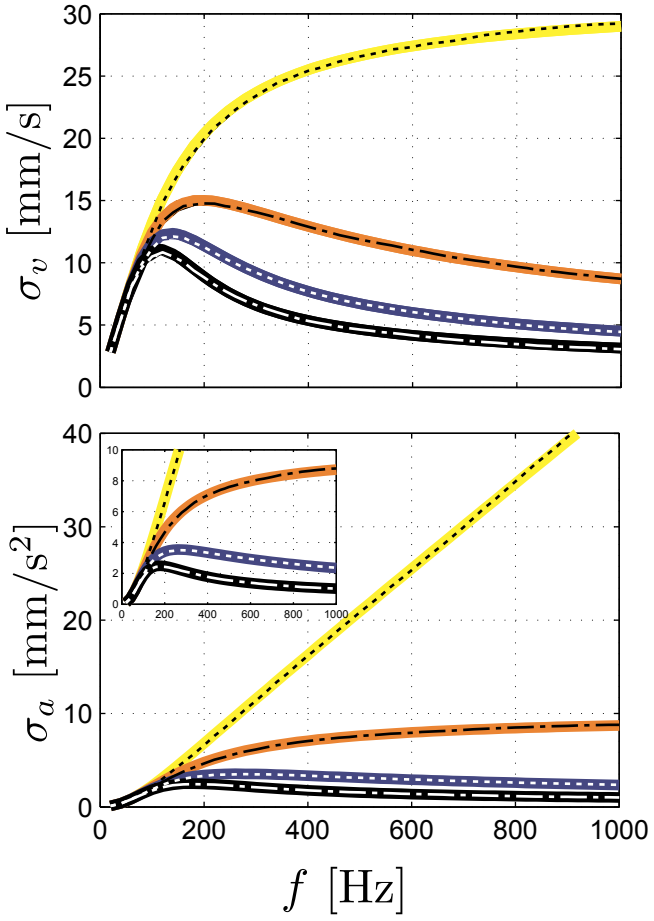

Fig. 9. The standard deviation of the error on velocity, σ_v, and acceleration, σ_a, plotted against the sample frequency f. There exists a relationship between the sample rate, the derivative signal order, d, and the order of the low-pass filter, n, which Table III summarize.

C. Frequency Response Intuition for Derivative Estimation Filters

A way to understand how the parameters of the derivative filter affect noise on the derivative signal is to examine the frequency response of the filter. The error on the derivative signal is the superposition of every error input through the filter at every frequency. Because the filters considered are discrete, this consists of constant zero-frequency signals up to the Nyquist frequency of the filter, $\omega_N = \pi/T$ [rad/s]. One way to eliminate error would be to have low, or even zero, magnitudes of the transfer function for all frequencies. Although this strategy would result in low error propagation, it would also result in a poor filter, in the sense that it would not estimate the derivative signal well. In practice, the filter designer's goal is to have high gain for signal frequencies, but low-gain for noise frequencies. For the IPQN model of quantization, the noise is white, meaning equal at all frequencies. The spectral content of quantization noise in more general cases in discussed in Appendix B.

Fig. 10 contains the frequency response for an acceleration filter, ($d = 2$), with filter orders n = 1, 2, 3, and 4, and a cut-off frequency of 50 [rad/s]. Also included is a schematic of

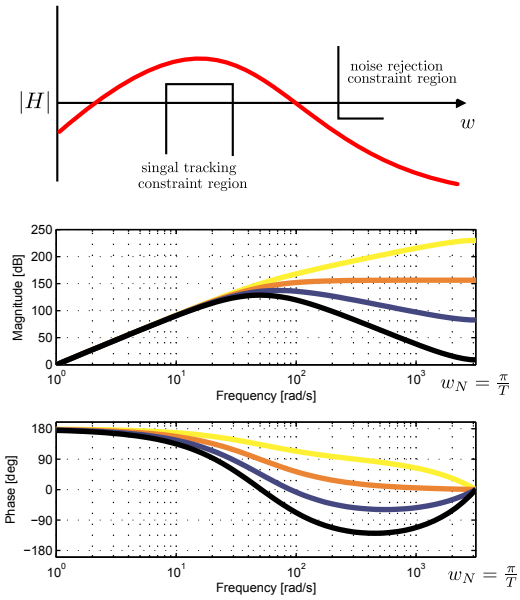

Fig. 10. The frequency response for an acceleration filter, ($d = 2$), with filter orders $n = 1 - 4$, and a cut-off frequency of 50 [rad/s], along with a schematic of the design goal for the magnitude of the frequency response.

the design goal for the magnitude of the frequency response. From the magnitude portion of the frequency response the qualitative effect of changing a filter parameters on the error can be determined. For example: if the cut-off frequency was made smaller, the frequency response would have a pole at a lower frequency and "roll-off" sooner, thus, the contribution of noise would be smaller. This is a classic and effective technique to develop filter designs [20].

VI. Experimental Verification

Experiments with a Phantom Premium (Sensable Inc.), as well as numerical simulations, were conducted to validate the theory presented. Two sets of experiments were performed. The first set analyzed the error distributions on operational space coordinates for various configurations of the robot from quantization in joint space. The second set tested the error distributions on operational space coordinate derivative signals. The joint and operational space coordinates of the robot are the standard coordinates for the Phantom Premium, and are shown schematically in Fig. 11.

A. Experimental Procedure

In both sets of experiments the robot was controlled to oscillate about a configuration with sinusoidal motion in which two types of signals were recorded: one with signals constructed from *artificially* quantized joint angles with a quantization interval of 1 milli-rad, and another without artificial quantization to create signals acting as truth. The amplitude of the motion, A, was $15°$, in each joint angle, and had a frequency, ω, of 2.5 Hz. The experiment was run at a control rate of 1 KHz, and a specific experiment was 15 seconds. The actual quantization

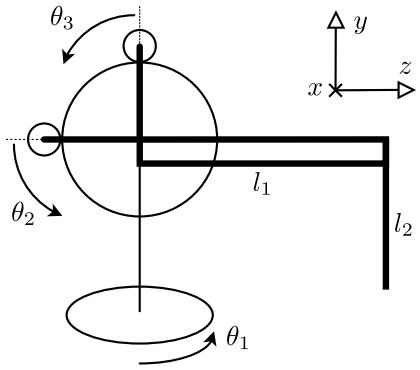

Fig. 11. The joint space coordinates: θ_1, θ_2, and θ_3 and operational space coordinates: x, y, and z. For the Phantom Premium 1.5, l_1 = 210 [mm], l_2 = 180 [mm], and a joint resolution of 0.125 milli-radians on all joints. The schematic displays the robot in the zero position. This figure is inspired from [21].

of the robot is 0.125 milli-rad. For all experiments, the value of Δf, was

$$\Delta f = (0.001 \text{ rad})(1000 \text{ Hz}) = 1 \text{ rad/s}. \tag{41}$$

The root-mean-square of the velocity, v_{RMS}, that the robot was controlled to follow in a joint was was

$$v_{\text{RMS}} = \frac{A\omega}{\sqrt{2}} = 3 \text{ rad/s} = 3\Delta f. \tag{42}$$

The numerical experiments were performed using Simulink using explicit quantization blocks.

B. Error Distribution on Operational Space Coordinates

The experimental error for an operational space coordinate, e.g. the x coordinate, was the difference between the signal constructed with artificial quantization and and the one without. The theoretical, simulated, and experimental standard deviations of the operational space coordinate errors are displayed in Fig. 12 for various configurations. Matching the prediction of theory, the mean of the experimental error was close to zero for all experiments. The largest magnitude of the mean for all experiments was than 2μm. Over all experiments the error was always within the bounds of Equation (17). The differences between the theory and experimental data present in Fig. 12 are discussed in Section VII.

C. Error Distribution on Operational Space Velocity and Acceleration

The error distribution on the velocity and acceleration of the x coordinate was tested for filter orders n = 1, 2, and 3 for various cut-off frequencies, f_0, of the low-pass filter about the zero position. The theoretical and experimental standard deviations of the operational space velocity and acceleration error are displayed in Fig. 13 for various cut-off frequencies. The mean of the experimental derivative error was small for all experiments as expected from theory: the largest magnitude of the mean of an error signal was less than 1% of its standard deviation for all experiments. The magnitude of all error values on the derivative signals was always within the bounds of

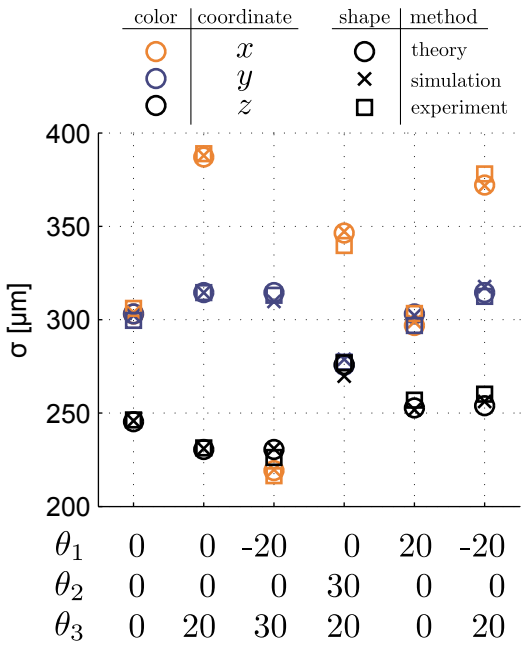

Fig. 12. The simulated and theoretical standard deviations of the operational space position error. The theoretical predications are essentially identical to the simulated results.

Equation (26). Additional experimental tests were conducted varying other filter parameters with similar results to matching theory. The simulated data are included as dotted lines in Figures 7, 8, and 9.

VII. Discussion

In Appendix B conditions for which the IPQN model of quantization is valid is presented. These conditions are based on the amplitude of motion in joint space compared to the quantization interval, $A \gg \Delta$, as well as the speed of the motion compared to the sampling rate, $v \gg \Delta f$. These conditions can also be expressed in operational space, for which some readers have more intuition. Instead of Δ in joint space, we can have Δ_x in operational space,

$$\Delta_x(\text{mm}) = \frac{l}{nG}. \tag{43}$$

$$\Delta_x f \left(\frac{\text{mm}}{\text{s}}\right) = \frac{lf}{nG}, \tag{44}$$

where n is the number of counts per revolution of the encoder, G is the gear ratio relating the quantized joint position to the abstract joint position, f is the sample frequency, and l is a characteristic "length" mapping a joint space coordinate to an operational space coordinate, i.e. an entry of the Jacobian in a certain configuration. For situations in which the quantization is directly on joint space G = 1. Table IV displays the values of Δ_x and $\Delta_x f$ for robots in common use today. Essentially all of the robots feature fine operational space resolution, and if the sample sample rate is sufficiently low, the conditions of IPQN are met to a high approximation. (I am finding it hard to find precise specifications for the robots. I have estimated some of the parameters,but I am confident this information is obtainable. I would also like to expand the list to around 10 robots with great "breath", specifically, I would like to feature a robot with a low Δ_x or high $\Delta_x f$.)

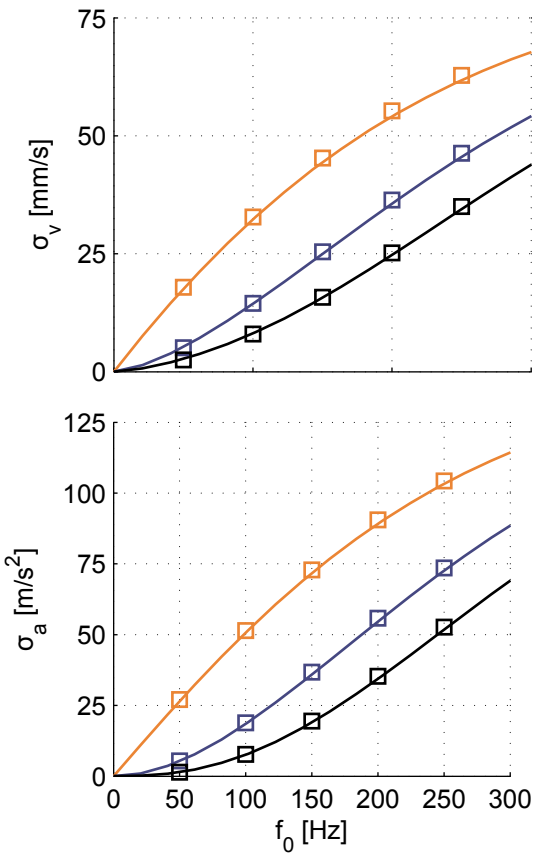

Fig. 13. Caption goes here.

TABLE IV
Robot Threshold Velocities

Robot units	n [tics/rev]	G [-]	l [mm]	f [Hz]	Δ_x [mm]	$\Delta_x f$ [mm/s]
Premium	2000	10	300	1000	.03	15.0
WAM (7dof)	nG = 3×10^6		500	1000	?	0.2
Kuka	nG = 1×10^6		500	1000	.05?	0.5
Omni	1000	5	100	1000	.055	10.0
Puma	2000	100	1000	1000	.01?	5

The theory presented has broad application, especially for design scenarios, but does have limitations. These limitations, which must be understood to apply the methods proposed, come from two main sources. The first source of limitation is that the IPQN model. The second limitation is that results for operational space and operational space derivative error are configuration dependent, and apply to a specific configuration. In many practical scenarios, the conditions of IPQN are satisfied to a good approximation, with no obvious interdependence among joint space coordinates, in which the quantization error in a certain region of the workspace where the forward kinematics are described reasonably well by an affine model, the sources of limitations are not important, but for others the limitations are.

These limitations explain the small departures from theory and experiment that is displayed in Fig. 12 and 13. In these experiments the motion of the robot spanned 15° in each joint, resulting in forward kinematics not perfectly described by a linear approximation, and motion with a root-mean-square velocity of $3\Delta f$ for which the error in joint space may have not been precisely uniform.

The theory presented for determining derivative error in section IV applies to all filters. The specific filter structure discussed for velocity and acceleration signals in section V was chosen to communicate the relationship between its parameters and the error on the derivative signals. The results for parameters of other filter structures, for which there exists a "cut-off frequency" and "order" in an abstract sense are similar. Butterworth filters in particular, are commonly used in real time low-pass filtering because continuous low-pass Butterworth filters feature a maximally flat passband and have good roll-off, and digital implementations can be easily obtained with a Bilinear transformation with pre-warping.

Fig. 9, Fig. 10, and Table III demonstrate that, practically speaking, to estimate a derivative signal of degree d, a filter of at least order n, and perhaps higher, is needed to limit noise propagation.

In this paper, the difference between the worst-case and stochastic results for joint and operational space coordinates is not that large, meaning, that one could probably bound the other within an order of magnitude. However, for the derivative signal errors the difference between the results can be very large. The stochastic results are only applicable when the IPQN model applies, so it seems that for conditions in which this is not true we don't have much to say about the derivative error. This is a moot point because when the IPQN model does not apply, FDM and low pass filters should not be used. Inverse time methods, "fixed-distance", are better suited in this position. Appendix A discusses this.

Nothing in the paper explicitly discussed joint spaced derivatives, but that is a subset of what was considered because in that case a identify Jacobian could be used.

In the A/D literature a technique called dither is used to make encoder noise more PQN, which makes analysis more easy. This technique has also been used in robotics to mitigate coulomb friction. Some short comments of this seem appropriate.

VIII. Conclusion

The main results of our analysis are the characterizations of encoder error in a robot system, i.e., given encoder specifications, robot kinematics, and a digital filter mapping an operational space coordinate to an estimate of its derivative, the effect of quantization error is described. The classic example of quantization error on velocity and acceleration signals for robot operational space coordinates is presented. Simulation and experimental data with a Phantom Premium support the theory presented. These results are intended as a design tool for robot kinematic and feedback control system design.

Appendix A
FDM and ITM Method Comparison

In this section two algorithms for estimating velocity from discrete quantized position are compared. The finite difference method, FDM, counts quantization "tics'' per unit time, and the inverse time method, ITM, counts the time elapsed between quantization tics. These algorithms are also called "fixed-time" and "fixed-distance" respectively. We establish conditions for which one algorithm outperforms the other with respect to its worst-case signal-to-noise-ratio, SNR. Specifically, for true velocity, v, quantization interval, Δ, and sample frequency f, in terms of the worst-case SNR, if

$$v < \Delta f \Rightarrow \text{ITM outperforms FDM}, \tag{45}$$

and if,

$$v > \Delta f \Rightarrow \text{FDM outperforms ITM}. \tag{46}$$

A. FDM Worst-Case SNR

For the FDM algorithm, the velocity error at time index k, v_k^e, is defined to be

$$v_k^e = v_k^t - v_k = \frac{x_k^t - x_{k-1}^t}{T} - \frac{x_k - x_{k-1}}{T} \tag{47}$$

where x_k^t and x_{k-1}^t are the current and one-sample-ago *true* positions, i. e. non-quantized positions, x_k and x_{k-1} are the current and one-sample-ago quantized with quantization interval Δ positions, and T is the sample period.

At a time step index k section IV establishes that the maximum difference between x_k^t and x_k is $\Delta/2$, therefore,

$$|v_k^e|_{\max} = \left| \frac{(x_k^t - x_k) + (x_{k-1}^t - x_{k-1})}{T} \right|_{\max} = \frac{\Delta}{T}. \tag{48}$$

The worst-case SNR for FDM is

$$\text{SNR}_{\text{FDM}} = \frac{v}{\Delta f}. \tag{49}$$

B. ITM Worst-Case SNR

The velocity error at encoder event index k for the ITM algorithm is defined to be

$$v_k^e = v_k^t - v_k = \frac{\Delta}{t_e^t - t_b^t} - \frac{\Delta}{t_e - t_b}, \tag{50}$$

where t_e^t and t_b^t are the *true* times in which the joint exits and begins the quantization interval, and t_e and t_b are the *detected* times in which the joint exits and begins the quantization interval. Because v_k^e is defined in this way, the velocity error is only defined at encoder events. Monotonic velocity within a quantization interval is assumed to yield a tractable maximum error. This eliminates pedantic cases in which the position of the joint oscillates in-between quantization "tics" in which the velocity goes positive and negative in which infinite error could occur.

Unlike FDM, v_k^e in the ITM algorithm depends on the velocity v. Let $v_{\max}$ be the velocity with the largest magnitude between two encoder events. Also, let the dimensionless

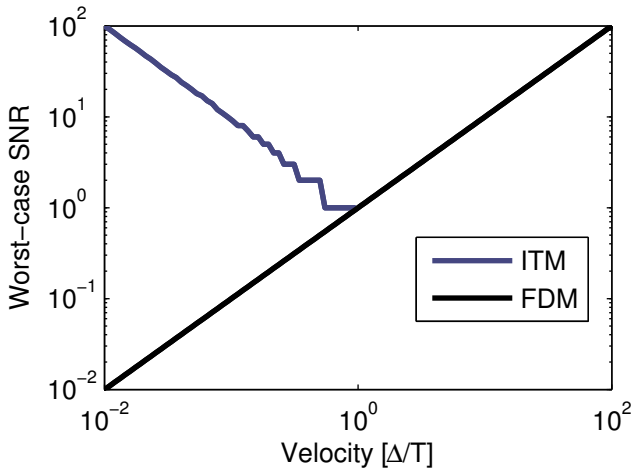

Fig. 14. Velocity versus SNR plot.

parameter $\alpha \in \mathbf{R}$ be the ratio of the top velocity that can be recored using ITM to the max velocity,

$$\alpha = \frac{\Delta f}{v_{\max}}. \tag{51}$$

Because the detected times between encoder events, $(t_e - t_b)$, must be a multiple of the sample times T, it is possible to bound $v_k^t - v_k$ in terms of the quantization interval and sample time,

$$|v_k^e|_{\max} = \frac{\Delta}{\lfloor \alpha \rfloor T}, \tag{52}$$

where $\lfloor \alpha \rfloor$ represents the floor of α. For values of $\alpha < 1$ the ITM method cannot guarantee that the distance between encoder tics is Δ. Therefore, the worst-case SNR for ITM is

$$\text{SNR}_{\text{ITM}} = \begin{cases} \frac{v}{\frac{\Delta}{\lfloor \alpha \rfloor T}} = \frac{v}{\frac{\Delta f}{\lfloor \alpha \rfloor}} & \text{if } \alpha \geq 1 \\ 0 & \text{if } \alpha < 1. \end{cases} \tag{53}$$

C. FDM and ITM Comparison

Figure 14 displays a plot of the worst-case SNR for the FDM and ITM algorithms plotted against velocity. Here the velocity is in units of the quantization interval over the sample rate: Δ/T. Expressed in these units, when the velocity is less than unity, the ITM algorithm has a higher worst-case SNR than FDM, and when velocity is greater than unity, the opposite is true.

APPENDIX B
IPQN CONDITIONS

A popular model for quantization noise is one of additive white noise uncorrelated to the input signal, uniformly distributed between plus and minus half the quantization interval. This model has been used extensively, despite the fact that quantization error is deterministically related to the to the input signal, and thus its distribution must also depend on the input signal.

Past researchers studying quantization for A/D applications such as [22], [23], and [24] have established precise conditions for when the pseudo-quantization noise, PQN, model is valid. Many of these results apply to modeling the input to the quantizer as a random variable, and the PQN model can be shown to be exact, or a very good approximation, based on qualities of the probability density function, or equivalently, the characteristic function, of the input.

For many robotic applications, where the input to the quantizer corresponds to joint space coordinates, the input is "smooth" in a certain sense, meaning it is locally correlated. Because of this, stochastic models for the input to the quantizer are not directly applicable. In addition to stochastic models, sine wave inputs have been studied. Sine inputs feature the type of "smoothness" that well characterize robotic joint space coordinates, and further, in general, a signal can be constructed from a combination of sine inputs, so this seems a better approach. Past studies have developed conditions to evaluate the validity of the PQN model for sine inputs. Put tersely, there are two conditions for when the PQN model *approximately*, meaning not exactly, holds. The first condition concerns the error distribution of the quantizer output. They found,

$$A \gg \Delta \Rightarrow \text{error is uniform.} \tag{54}$$

With the precise statement being that the largest possible difference for the mean of a quantized sine wave with with peak velocity v, amplitude A, and frequency f_i, over *all* DC offsets and PQN, (what the literature calls Sheppard's first correction, R1), is inside the envelope,

$$R1 \pm \frac{0.135\Delta}{\sqrt{A/\Delta}}. \tag{55}$$

The largest possible difference for the variance of a quantized sine wave over *all* DC offsets and PQN, (what the literature calls Sheppard's second correction, R2), is inside the envelope

$$\frac{\Delta^2}{12} - 0.029\frac{\Delta^2}{\sqrt{A/\Delta}} < R2 < \frac{\Delta^2}{12} + 0.038\frac{\Delta^2}{\sqrt{A/\Delta}}. \tag{56}$$

The second condition concerns the correlation of the noise, (or the whiteness) of the spectrum. Here the condition for a sine wave with peak velocity v, amplitude A, and frequency f_i, with sample frequency f, is

$$v \gg \Delta f \Rightarrow \text{error is white.} \tag{57}$$

With the precise statement being that the condition

$$(1/2)\pi A > \Delta f, \tag{58}$$

ensures that 95% of the power of the quantization error is white.

Note that these values are worst case over all mu. With respect to the current problem the average case, meaning the average correction value over all mu values, and perhaps even weighted by the amplitude makes the most sense, but I don't know if results on this exist.

The resulting spectrum will contain some ripples for any value of f, but the power of them will be small compared to the power of the quantization noise.

These results come from [24], and were originally found by [25].

The last assumption for IPQN is that each quantization source is independent of the others. Precise conditions, as well as approximate conditions exist as well, but this one seems application specific in robotics.

REFERENCES

[1] H. Tanaka, H. Nishi, and K. Ohnishi, "An approach to acceleration estimation using fpga," in *Industrial Electronics, 2008. ISIE 2008. IEEE International Symposium on*, 2008, pp. 1959–1964.

[2] A. J. Harrison and C. A. McMahon, "Estimation of acceleration from data with quantization errors using central finite-difference methods," *Proceedings of the Institution of Mechanical Engineers, Part I: Journal of Systems and Control Engineering*, vol. 207, no. 2, pp. 77–86, 1993. [Online]. Available: http://pii.sagepub.com/content/207/2/77.abstract

[3] A. J. L. Harrison and D. P. Stoten, "Generalized finite difference methods for optimal estimation of derivatives in real-time control problems," *Proceedings of the Institution of Mechanical Engineers, Part I: Journal of Systems and Control Engineering*, vol. 209, no. 2, pp. 67–78, 1995. [Online]. Available: http://pii.sagepub.com/content/209/2/67.abstract

[4] R. Kavanagh and J. M. D. Murphy, "The effects of quantization noise and sensor nonideality on digital differentiator-based rate measurement," *Instrumentation and Measurement, IEEE Transactions on*, vol. 47, no. 6, pp. 1457–1463, 1998.

[5] G. Mollova, "Variance of quantization error at the output of recursive digital filter," in *Signals, Systems, and Electronics, 1995. ISSSE '95, Proceedings., 1995 URSI International Symposium on*, 1995, pp. 439–442.

[6] S. M. Phillips and M. S. Branicky, "Velocity estimation using quantized measurements," *Proc. IEEE Conf. on Decision and Control, Maui*.

[7] R. Merry, M. van de Molengraft, and M. Steinbuch, "Velocity and acceleration estimation for optical incremental encoders," *Mechatronics*, vol. 20, no. 1, pp. 20 – 26, 2010.

[8] T. Tsuji and H. Kobayashi, "Robust acceleration control based on acceleration measurement using optical encoder," in *Industrial Electronics, 2007. ISIE 2007. IEEE International Symposium on*, 2007, pp. 3108–3113.

[9] P. R. Belanger, P. Dobrovolny, A. Helmy, and X. Zhang, "Estimation of Angular Velocity and Acceleration from Shaft-Encoder Measurements," *International Journal of Robotic Research*, vol. 17, pp. 1225–1233, 1998.

[10] S. C. Armando Bellini, Stefano Bifaretti, "A digital speed filter for motion control drives with a low resolution position encoder."

[11] J. Zhou, X. Shen, E. Petriu, and N. Georganas, "Linear velocity and acceleration estimation of 3 dof haptic interfaces," in *Haptic Audio visual Environments and Games, 2008. HAVE 2008. IEEE International Workshop on*, oct. 2008, pp. 137 –142.

[12] G. Liu, "On velocity estimation using position measurements," in *American Control Conference, 2002. Proceedings of the 2002*, vol. 2, 2002, pp. 1115 – 1120 vol.2.

[13] M. M. A. Tilli, "A low-noise estimator of angular speed and acceleration from shaft encoder measurements," *Journal Automatika*.

[14] O. Baser, E. Kilic, E. Konukseven, and M. Dolen, "A hybrid method to estimate velocity and acceleration using low-resolution optical incremental encoders," in *Signals and Electronic Systems (ICSES), 2010 International Conference on*, sept. 2010, pp. 57 –60.

[15] S. D"Arco, L. Piegari, and R. Rizzo, "An optimised algorithm for velocity estimation method for motor drives," in *Diagnostics for Electric Machines, Power Electronics and Drives, 2003. SDEMPED 2003. 4th IEEE International Symposium on*, 2003, pp. 76–80.

[16] F. Janabi-Sharifi, V. Hayward, and C.-S. Chen, "Discrete-time adaptive windowing for velocity estimation," *Control Systems Technology, IEEE Transactions on*, vol. 8, no. 6, pp. 1003 –1009, nov 2000.

[17] A. Y. Barraud, "A numerical algorithm to solve at x a - x = q," in *Decision and Control including the 16th Symposium on Adaptive Processes and A Special Symposium on Fuzzy Set Theory and Applications, 1977 IEEE Conference on*, vol. 16, 1977, pp. 420–423.

[18] R. H. Bartels and G. W. Stewart, "Solution of the matrix equation ax + xb = c [f4]," *Commun. ACM*, vol. 15, no. 9, pp. 820–826, Sep. 1972. [Online]. Available: http://doi.acm.org/10.1145/361573.361582

[19] G. Golub, S. Nash, and C. Van Loan, "A hessenberg-schur method for the problem ax + xb= c," *Automatic Control, IEEE Transactions on*, vol. 24, no. 6, pp. 909–913, 1979.

[20] G. F. Franklin, D. J. Powell, and A. Emami-Naeini, *Feedback Control of Dynamic Systems*, 4th ed. Upper Saddle River, NJ, USA: Prentice Hall PTR, 2001.

[21] M. C. avusoglu, M. C. avusoglu, D. Feygin, and F. Tendick, "A critical study of the mechanical and electrical properties of the phantom haptic interface and improvements for high performance control," *Presence*, vol. 11, pp. 555–568, 2002.

[22] W. R. Bennett, "Spectra of quantized signals," *Bell System Technical Journal*, vol. 27, no. 4, pp. 446–472, Jul 1948.

[23] A. B. Sripad and D. L. Snyder, "A necessary and sufficient condition for quantization errors to be uniform and white," vol. 25, no. 5, pp. 442–448, Oct 1977.

[24] B. Widrow and I. Kollár, *Quantization Noise: Roundoff Error in Digital Computation, Signal Processing, Control, and Communications*. Cambridge, UK: Cambridge University Press, 2008.

[25] I. Kollár, "Bias of mean value and mean square value measurements based on quantized data," vol. 43, no. 5, pp. 733–9, Oct 1994.